Potential energy surface and wave packet calculations on the Li+HF → LiF+H reaction

Alfredo Aguado, Miguel Paniagua, Manuel Lara, and Octavio Roncero

Citation: The Journal of Chemical Physics **106**, 1013 (1997); doi: 10.1063/1.473185
View online: http://dx.doi.org/10.1063/1.473185
View Table of Contents: http://scitation.aip.org/content/aip/journal/jcp/106/3?ver=pdfcov
Published by the AIP Publishing

Potential energy surface and wave packet calculations on the Li+HF→LiF+H reaction

Alfredo Aguado and Miguel Paniagua
Departamento de Química Física, Facultad de Ciencias C–XIV, Universidad Autónoma de Madrid, 28049 Madrid, Spain

Manuel Lara and Octavio Roncero
Instituto de Matemáticas y Física Fundamental, C.S.I.C., Serrano 123, 28006 Madrid, Spain

(Received 19 July 1996; accepted 2 October 1996)

In this work an analytic fit of previous *ab initio* points [Aguado, Suárez, and Paniagua, Chem. Phys. **201**, 107 (1995)] on the potential energy surface of the LiFH system is presented and the reaction dynamics is studied using a time-dependent treatment based on local coordinates. Three-dimensional wave packet calculations performed for zero total angular momentum indicate that the reactivity for the HF reactant in its ground vibrational state is quite low, in contradiction with previous dynamical calculations using different potential energy surfaces. The differences with previous potential energy surfaces are further analyzed using a bidimensional approach. Finally, the effect of the initial vibrational excitation of the HF reactant on the reactivity is studied using the bidimensional approach. © *1997 American Institute of Physics.* [S0021-9606(97)01502-X]

I. INTRODUCTION

The M+HX→MX+H (M=alkali metal, X=halogen) elementary reactions have attracted much attention from the first crossed molecular beam experiment performed by Taylor and Datz.[1] The study of the state-to-state reaction

$$\mathrm{Li+HF}(v_1,\ell_1)\rightarrow\mathrm{LiF}(v_2,\ell_2)+\mathrm{H} \tag{1}$$

is the simplest case on this kind of systems. Due to its relative simplicity this reaction has recently attracted the attention of both theoreticians and experimentalists and it is becoming a benchmark system to study elementary reactions. The first crossed beam experiments on this system were performed by Lee and co-workers.[2] More recently the influence of the initial vibrational excitation of the reactants was studied by using an infrared laser to excite the HF molecule.[3–6] Moreover, by introducing an electric field it was possible to study the influence of the reagents relative orientation.[4,6]

An additional interest of this kind of system is that they usually fulfill a set of conditions for photon catalysis.[7–13] An increasing number of studies have been performed since the pioneering work of Soep,[14,15] Wittig[16] and their co-workers on photoinduced chemical reactions occurring in van der Waals complexes. In this experiment a weakly bonded complex of the reactants is formed in a supersonic beam expansion and it is promoted to an excited electronic state where the reaction takes place. Finally, the products are analyzed using different spectroscopic techniques. In these experiments the orientation between the fragments is fixed within the complex and the laser excitation permits a study of the reaction at very well determined energy conditions. The study of the intermediate species using short laser pulse techniques provides direct information on the reaction mechanisms. The LiFH system is a good candidate for such studies since it has a relatively deep well in the entrance channel[6] and recent *ab initio* calculations on excited electronic states[17] indicate that the optical excitation is in the near-infrared to visible spectral range. In fact, several photoinduced chemical reactions[14,15] experiments have been recently carried out on this system[18] or related, such as CaHF.[19]

The potential energy surface (PES) of the ground electronic state of LiFH has been calculated using semiempirical,[20–22] density functional[23,24] and *ab initio*[17,25–27] methods and there are several fits of the PES.[28–32] The Li+HF reactive collision has been studied using classical trajectories[33,34] and quantum calculations, with reduced dimensionality approaches[35] and three-dimensional treatments[32,36,37] using, in most of cases, the PES of Ref. 32 or previous versions of the same PES.[29,30]

In this work we present a new fit to the most recent and accurate *ab initio* energy points.[17] The quantum reactive dynamics is studied using a three-dimensional time-dependent method based on local coordinates which allows us to describe reactants and products at the same time but which requires the inclusion of kinetic crossing terms. The previous quantum time-dependent study[37] on this system was performed using reactants and products Jacobi coordinates which requires consideration of the coordinates transformation. In the present treatment such transformation is avoided, provided that the kinetic crossing term is neglected in the asymptotic regions. To analyze the importance of the PES features, such as the height and shape of the transition state, time-dependent calculations on three different PES are performed using a two-dimensional approach. In addition, the effect of the vibrational excitation of the HF reactant is studied using the reduced dimensionality approach. The paper is organized as follows. In Section II the time-dependent quantum treatment is presented. The details of the fit of the PES are described in Section III and the results of the dynamical calculations are discussed in Section IV. Finally, Section V is devoted to the conclusions.

II. TIME-DEPENDENT REACTIVE SCATTERING THEORY

Nowadays, reactant Jacobi coordinates are widely used in time-dependent studies on atom-diatom,[38,39] diatom-diatom[40–43] and atom-triatom[44] collisions to obtain total reaction probabilities. To extract state-to-state information it is necessary to propagate the initial wave packet into the interaction region, transform it to the product Jacobi coordinates[37,38] and then the propagation is continued and its final states are analyzed. To overcome this difficulty for the reaction under study, in Eq. (1), both reactants and products are described in terms of local coordinates defined by the position vectors $\mathbf{R}_1$ and $\mathbf{R}_2$ of H and Li atoms, respectively, with respect to the central F atom. The Hamiltonian expressed in these coordinates becomes

$$H=-\frac{\hbar^2}{2\mu_1}\left(\frac{\partial^2}{\partial R_1^2}+\frac{2}{R_1}\frac{\partial}{\partial R_1}\right)+\frac{\hbar^2\mathbf{l}_1{}^2}{2\mu_1R_1^2}-\frac{\hbar^2}{2\mu_2}\left(\frac{\partial^2}{\partial R_2^2}+\frac{2}{R_2}\frac{\partial}{\partial R_2}\right)+\frac{\hbar^2\mathbf{l}_2{}^2}{2\mu_2R_2^2}-\frac{\hbar^2}{m_F}\nabla_1\cdot\nabla_2+V_{ABC}(\mathbf{R}_1,\mathbf{R}_2), \tag{2}$$

where $\mu_1=m_{\mathrm{H}}m_{\mathrm{F}}/(m_{\mathrm{H}}+m_{\mathrm{F}})$, $\mu_2=m_{\mathrm{Li}}m_{\mathrm{F}}/(m_{\mathrm{Li}}+m_{\mathrm{F}})$ and $\mathbf{l}_i$ are the angular momenta associated to $\mathbf{R}_i$, $i=1,2$, with $\mathbf{J}=\mathbf{l}_1+\mathbf{l}_2$ being the total angular momentum. This Hamiltonian has been widely used for the calculation of rovibrational states of triatomic molecules[45–49] and more recently of tetra-atomic van der Waals clusters.[50] It has also been used for the study of photodissociation of symmetric triatomic molecules.[51–54] For these coordinates the kinetic crossing term, $\nabla_1\cdot\nabla_2$, does not vanish for large R_1 or R_2 distances, since it accounts for the differences between Jacobi and local coordinates in the asymptotic regions. Therefore, the final state of the fragments, in particular their kinetic energy distribution, are not properly described unless a transformation to the adequate Jacobi coordinates is performed. In this work this term is included in the dynamical calculations, since it is important at short distances. However, in the asymptotic region the transformation to Jacobi coordinates is not performed since it is expected to have a small contribution there, as will be discussed later.

The quantum dynamics is described by the evolution in time of a wave packet expressed as

$$\Psi^{JM}(\mathbf{R}_1,\mathbf{R}_2,t)=\sum_{\ell_1\ell_2}\frac{\Phi^{JM}_{\ell_1\ell_2}(R_1,R_2,t)}{R_1R_2}\mathscr{W}^{JM}_{\ell_1\ell_2}(\hat{\mathbf{R}}_1,\hat{\mathbf{R}}_2) \tag{3}$$

with the angular functions being defined in the space-fixed frame as,

$$\mathscr{W}^{JM}_{\ell_1\ell_2}(\hat{\mathbf{R}}_1,\hat{\mathbf{R}}_2)=(-1)^{\ell_1-\ell_2+M}\sqrt{2J+1}\sum_{m_1m_2}\begin{pmatrix}\ell_1 & \ell_2 & J\\ m_1 & m_2 & -M\end{pmatrix}\times Y_{\ell_1m_1}(\hat{R}_1)Y_{\ell_2m_2}(\hat{R}_2), \tag{4}$$

where $(\vdots)$ denotes $3-j$ symbols and $Y_{\ell_im_i}(\theta_i,\phi_i)$ are spherical harmonics.

The radial $\Phi^{JM}_{\ell_1\ell_2}(R_1,R_2,t)$ coefficients in Eq. (3) contain the information of the dynamics and satisfy the set of coupled equations,

$$\begin{aligned}i\hbar\frac{\partial}{\partial t}\Phi^{JM}_{\ell_1\ell_2}(R_1,R_2,t)&=\left\{-\frac{\hbar^2}{2\mu_1}\frac{\partial^2}{\partial R_1^2}-\frac{\hbar^2}{2\mu_2}\frac{\partial^2}{\partial R_2^2}+\frac{\hbar^2\ell_1(\ell_1+1)}{2\mu_1R_1^2}+\frac{\hbar^2\ell_2(\ell_2+1)}{2\mu_2R_2^2}\right\}\Phi^{JM}_{\ell_1\ell_2}(R_1,R_2,t)\\&+\sum_{\ell_1'\ell_2'}\left\langle\mathscr{W}^{JM}_{\ell_1\ell_2}\middle|V(\mathbf{R}_1,\mathbf{R}_2)-\frac{\hbar^2}{m_F}\mathscr{D}_{12}\middle|\mathscr{W}^{JM}_{\ell_1'\ell_2'}\right\rangle\Phi^{JM}_{\ell_1'\ell_2'}(R_1,R_2,t),\end{aligned} \tag{5}$$

where $\mathscr{D}_{12}$ has been defined to satisfy

$$\nabla_1\cdot\nabla_2\frac{\Phi^{JM}_{\ell_1\ell_2}(R_1,R_2,t)}{R_1R_2}=\frac{1}{R_1R_2}\mathscr{D}_{12}\Phi^{JM}_{\ell_1\ell_2}(R_1,R_2,t)$$

so that the kinetic coupling matrix elements are written as[50]

$$\begin{aligned}\langle\mathscr{W}^{JM}_{\ell_1\ell_2}|\mathscr{D}_{12}|\mathscr{W}^{J'M'}_{\ell_1'\ell_2'}\rangle&=\delta_{JJ'}\delta_{MM'}\delta_{\ell_1'\ell_1\pm1}\delta_{\ell_2'\ell_2\pm1}(-1)^{J+\ell_1+\ell_2'}\\&\times\sqrt{\ell_1^{\max}\ell_2^{\max}}\begin{Bmatrix}\ell_2 & \ell_2' & 1\\ \ell_1' & \ell_1 & J\end{Bmatrix}\\&\times\left\{(-1)^{s_1+s_2}\frac{\partial^2}{\partial R_1\partial R_2}-(-1)^{s_1}\frac{\ell_2^{\max}}{R_2}\frac{\partial}{\partial R_1}\right.\\&\left.-(-1)^{s_2}\frac{\ell_1^{\max}}{R_1}\frac{\partial}{\partial R_2}+\frac{\ell_1^{\max}\ell_2^{\max}}{R_1R_2}\right\},\end{aligned} \tag{6}$$

where $\ell_i^{\max}=\max(\ell_i\ell_i')$ and $s_i=1$ for $\ell_i^{\max}=\ell_i'$ and zero elsewhere, and $(\vdots)$ denotes $6-j$ symbols.

Finally, the potential matrix elements in Eq. (5), take the form,[50]

$$\begin{aligned}\langle\mathscr{W}^{JM}_{\ell_1\ell_2}|V|\mathscr{W}^{JM}_{\ell_1'\ell_2'}\rangle&=\delta_{JJ'}\delta_{MM'}(-1)^{J-\ell_2-\ell_2'}\\&\times\sqrt{(2\ell_1+1)(2\ell_1'+1)(2\ell_2+1)(2\ell_2'+1)}\\&\times\sum_\Lambda V_\Lambda(R_1,R_2)\begin{Bmatrix}\ell_1' & \ell_1 & \Lambda\\ \ell_2 & \ell_2' & J\end{Bmatrix}\begin{pmatrix}\ell_1 & \Lambda & \ell_1'\\ 0 & 0 & 0\end{pmatrix}\\&\times\begin{pmatrix}\ell_2 & \Lambda & \ell_2'\\ 0 & 0 & 0\end{pmatrix},\end{aligned} \tag{7}$$

where $V_\Lambda(R_1,R_2)$ are the coefficients of a Legendre expansion of the potential, i.e.,

$$V(R_1,R_2,\cos\theta)=\sum_\Lambda V_\Lambda(R_1,R_2)P_\Lambda(\cos\theta) \tag{8}$$

with $\cos\theta=\mathbf{R}_1\cdot\mathbf{R}_2/R_1R_2$.

The decomposition of the wave packet in terms of the asymptotic states of the fragments gives an idea of how the collision proceeds, and when the two fragments are well separated the quantities defined as

$$\begin{aligned}P^{\mathrm{HF}}_{v_1\ell_1}(t)&=\sum_{\ell_2}\int dR_2\left|\int dR_1\ \phi^{\mathrm{HF}*}_{v_1\ell_1}(R_1)\right.\\&\quad\left.\times\Phi^{JM}_{\ell_1\ell_2}(R_1,R_2,t)\right|^2\\P^{\mathrm{LiF}}_{v_2\ell_2}(t)&=\sum_{\ell_1}\int dR_2\left|\int dR_1\ \phi^{\mathrm{LiF}*}_{v_2\ell_2}(R_2)\right.\\&\quad\left.\times\Phi^{JM}_{\ell_1\ell_2}(R_1,R_2,t)\right|^2\end{aligned} \tag{9}$$

correspond to the rovibrational populations of the diatomic fragments. In Eqs. (9), $\phi^{\mathrm{HF}}_{v_1\ell_1}(R_1)$ and $\phi^{\mathrm{LiF}}_{v_2\ell_2}(R_2)$ are the solutions of the radial Schrödinger equations, for HF reactants

$$\left\{-\frac{\hbar^2}{2\mu_1}\frac{d^2}{dR_1^2}+\frac{\hbar^2}{2\mu_1R_1^2}\ell_1(\ell_1+1)+V_{\mathrm{HF}}(R_1)-E_{v_1\ell_1}\right\}\phi_{v_1\ell_1}(R_1)=0 \tag{10}$$

and LiF products,

$$\left\{-\frac{\hbar^2}{2\mu_2}\frac{d^2}{dR_2^2}+\frac{\hbar^2}{2\mu_2R_2^2}\ell_2(\ell_2+1)+V_{\mathrm{LiF}}(R_2)-E_{v_2\ell_2}\right\}\phi_{v_2\ell_2}(R_2)=0, \tag{11}$$

respectively.

The initial wave packet corresponds to a specific $(v_1^0\ell_1^0)$ eigenstate of HF and it is described by the product,

$$\Psi^{JM}(\mathbf{R}_1,\mathbf{R}_2,t=0)=\frac{\phi_{v_1^0\ell_1^0}(R_1)}{R_1}\frac{G(R_2)}{R_2}W^{JM}_{\ell_1^0\ell_2}(\hat{R}_1,\hat{R}_2), \tag{12}$$

where $G(R)$ is a complex Gaussian,

$$G(R)=\left(\frac{2}{\pi\gamma^2}\right)^{1/4}\exp\left[-\frac{(R_2-R_2^0)^2}{\gamma^2}-ik^0R_2\right] \tag{13}$$

centered at an initial value R_2^0 in the asymptotic region and with an approximated mean initial kinetic energy of $\hbar^2(k^0)^2/2\mu_2$, where γ is related to the width of the energy distribution.

At sufficiently long time the wave packet describes two free particles flying apart in well determined eigenstates of the different rearrangement fragments, so that it can be expressed as,

$$\begin{aligned}&\Psi^{JM}(\mathbf{R}_1,\mathbf{R}_2,t\to\infty)\\&=\sum_{\ell_1\ell_2}\left\{\sum_{v_1}\int dk_2\ C_{v_1\ell_1\ell_2}(k_2,t)\phi^{\mathrm{HF}}_{v_1\ell_1}(R_1)e^{ik_2R_2}\right.\\&\quad+\sum_{v_2}\int dk_1\ C_{v_2\ell_1\ell_2}(k_1,t)\phi^{\mathrm{LiF}}_{v_2\ell_2}(R_2)\\&\quad\left.\times e^{ik_1R_1}\right\}W^{JM}_{\ell_1\ell_2}(\hat{R}_1,\hat{R}_2),\end{aligned} \tag{14}$$

where the kinetic crossing term in Eq. (2) is neglected in the asymptotic region. The energy dependence of the reaction probability on a particular final state of the fragments, (v_α,ℓ_α with $\alpha=1,2$ for HF or LiF fragments, respectively), from the specified initial reactant level (v_1^0,ℓ_1^0) is then given by the **S** matrix elements by[55]

$$\begin{aligned}P_{v_\alpha,\ell_\alpha}(E)&=|S_{v_\alpha,\ell_\alpha,v_1^0,\ell_1^0}(E)|^2\\&=\frac{\mu_\alpha k_{v_1^0,\ell_1^0}}{\mu_2 k_{v_\alpha,\ell_\alpha}}\left|\frac{C_{v_\alpha,\ell_\alpha}(k_{v_\alpha,\ell_\alpha},t\to\infty)}{\langle e^{-ik^0_{v_1^0,\ell_1^0}R_2}|G(R_2)\rangle}\right|^2,\end{aligned} \tag{15}$$

where $\mu_\alpha=\mu_2,\mu_1$ for $\alpha=1,2$, respectively, and $k_{v_\alpha,\ell_\alpha}=\sqrt{2\mu_\alpha(E-E_{v_\alpha,\ell_\alpha})}/\hbar$. [In Eq. (15) only ℓ_α is used instead of ℓ_α,ℓ_β to simplify the notation.]

The wave packet spreads in time over a very large spatial region and it is convenient to separate those contributions arriving to very large distances where the propagation may be done analytically using the free particle propagator in the momentum space. For that purpose the total wave packet is split as $\Psi(t)=\Psi_I(t)+\Psi_P(t)$, where $\Psi_I(t)$ is non-zero in the interaction region, while $\Psi_P(t)$ is in the asymptotic region.[56,57] $\Psi_I(t)$ is described as in Eq. (3) in a radial grid of size L. The initial wave packet is located in the interaction region which requires the use of a sufficiently large radial grid to consider a portion of the region where the reactants do not interact. At sufficiently long times the wave packet describes fragments flying apart at very large distances and $\Psi_P(t\to\infty)$ is expressed in terms of the asymptotic solutions of the Hamiltonian, as in Eq. (14). The steps followed at each time interval of the propagation of the total wave packet are

- $\Psi_I(t)$ is propagated by solving Eq. (5) using the Chebyshev method.[58] $\Psi_P(t)$ is propagated analytically using the free particle propagator in the momentum space and neglecting the kinetic crossing term.
- Each $\Psi_I(t)$ to be used in the next time step is replaced by $\Psi_I(t)f_1(R_1)f_2(R_2)$, where $f_i(R_i)=\exp[-\beta_i(R_i-R_i^{\mathrm{abs}})^2]$ if $R_i>R_i^{\mathrm{abs}}$ and $f_i(R_i)=1$ otherwise. This procedure, usually called absorption, requires a careful choice of parameters to avoid artificial reflections, due to the use of finite radial grids, and to minimize its effect on the wave packet.
- The probability thus absorbed, $\Psi_I(t)[1-f_1(R_1)f_2(R_2)]$, is expressed as in Eq. (14) and added to $\Psi_P(t)$ to form the new asymptotic wave packet for the next time step. This procedure requires the projection of $\Psi_I(t)[1-f_1(R_1)f_2(R_2)]$ on the final states of the

diatomic fragments and the radial coefficients thus obtained, which depend either on R_1 or on R_2, are transformed to the momentum domain using the FFT algorithm.[59] Since $\Psi_J(t)$ is described in a radial interval of length L, the momentum resolution is given by $2\pi/L$. In order to improve the momentum resolution, this last transformation is performed in a much larger grid of length $N\times L$ using the same radial step[56] (since the absorbed probability is well located in the absorption region it may be considered to be zero elsewhere). This procedure is applied to monodimensional radial grids for particular final states of the rearrangement fragments and does not increase the computational effort as compared to the propagation of $\Psi_J(t)$.

III. POTENTIAL ENERGY SURFACE

The starting point for the construction of a PES is a set of electronic energy values over a wide domain of the configuration space. The LiFH electronic energy has been calculated using semiempirical,[20–22] density functional[23,24] and *ab initio*[17,25–27] methods. These calculations reveal that the PES has a nonlinear transition state shifted into the exit channel (except for Ref. 20). The predicted barrier height goes from 0.250 eV[17] to 0.555 eV.[23] The first LiFH PES reported by Lester and Krauss[25] noted the presence of an attractive well or Li···FH complex located in the reactants side, that deepens slightly away from collinearity. The predicted complex binding energy goes from -0.498 eV[24] to -0.095 eV,[22] with respect to the zero energy at the reactants. If we consider only the *ab initio* configuration interaction (CI) calculations as the most accurate ones, the predicted barrier height goes from 0.250 eV[17] (multireference CI calculation, or MRDCI) to 0.433 eV[26] (CI with only one reference configuration, or CISD) and the complex binding energy goes from -0.290 eV[17] (MRDCI) to -0.199 eV[26] (CISD).

The results of Ref. 26 (CISD) have been fitted to different analytical forms.[28,31,32] However, despite the fact that these fits are based on the same *ab initio* data, they result in very different potentials. The reason is that only one of them is a true *ab initio* PES[31] (hereafter referred to as PES1), i.e., without *ad hoc* modifications or adjustments such as the ''addition of a few graphically extrapolated points''[28] to reproduce the LiF+H asymptote and the experimental exothermicity, the ''subtraction of Gaussian functions centered at the transition state''[28,32] to modify the barrier height that was judged to be too high, the ''scaling of the data points''[28,32] to reproduce experimental data, the ''subtraction of 0.01561 Å from all HF distances and 0.04113 Å from all LiF distances''[28] to obtain an agreement between experimental and calculated diatomic bond lengths, the ''scaling of the three-body coefficients by the factor 0.9935''[32] to ''fine tune'' the characteristics of the stationary points. Therefore, we refer to these latter PES as *ad hoc* PES; the most recent one being that by Parker *et al.* PES[32] (hereafter referred to as PES2). Obviously, this is not an only way to obtain *ad hoc* PES's because they are based in part in experimental data and theoretical data, and in part in judgments about experimental and theoretical results.

Here, we present the PES fit (in the *ab initio* sense) corresponding to the ground state of the LiFH system using the most accurate MRDCI adiabatic energies,[17] recently reported. The lowest excited state presents an avoided crossing with respect to the ground state. The characterization of the crossing region is very difficult due to a strong adiabatic coupling in LiFH, but its position is close to the ground-state saddle region.[27] At present we are trying to fit the adiabatic lowest excited-state, that will be presented elsewhere.

The LiFH adiabatic potential corresponding to the $^2A'$ ground state is fitted by means of the same global fitting procedure used for our previous fit[31] to the *ab initio* points of Chen and Schaefer III.[26] This procedure is based on the many-body expansion[60]

$$V_{ABC}=\sum_A V_A^{(1)}+\sum_{AB} V_{AB}^{(2)}(R_{AB}) + V_{ABC}^{(3)}(R_{AB},R_{AC},R_{BC}), \tag{16}$$

where the summations run over all the terms of a given type and where $V_A^{(1)}$ is the energy of atom A in its appropriate electronic state; usually, we adopt $\Sigma_A V_A^{(1)}=0$ for all the atoms in their ground state. $V_{AB}^{(2)}$ is the two-body energy, that is expressed using a polynomial form[31]

$$V_{AB}^{(2)}=\frac{c_0 e^{-\alpha_{AB}R_{AB}}}{R_{AB}}+\sum_{i=1}^{N} c_i\rho_{AB}^i, \tag{17}$$

the polynomial Rydberg type variables ρ are given by

$$\rho_{AB}=R_{AB}e^{-\beta_{AB}^{(\ell)}R_{AB}},\ \ell=2(\text{two-body})\ \text{ or }\ 3(\text{three-body}). \tag{18}$$

The linear parameters c_i, $i=0,1,\ldots,N$ and the nonlinear parameters α_{AB} and $\beta_{AB}^{(2)}$ are determined by fitting the *ab initio* values corresponding to the ground states of the diatomic fragments (plus separated atom at large enough distance) computed with the same basis set as for the triatomic system and using the same *ab initio* procedure. In Table I we present the parameters obtained for the fits of the diatomic fragments. The diatomic vibrational eigenvalues for HF, LiF and LiH, listed in Table II, show that the reaction Li + HF → LiF + H is classically endoergic but quantally exoergic when the zero-point energy is included, as was the case of previous PES.[28,31,32] We can also see from this table that the reaction Li + HF → LiH + F is endoergic both classically and quantally being energetically very unfavorable.

The three-body term $V_{ABC}^{(3)}$ of the potential in Eq. (16) is also expressed as a polynomial of order M in the same variables ρ_{AB}, ρ_{AC} and ρ_{BC} [see Eq. (18) with $\ell=3$]

$$V_{ABC}^{(3)}(R_{AB},R_{AC},R_{BC})=\sum_{i,j,k}^{M} d_{ijk}\rho_{AB}^i\rho_{AC}^j\rho_{BC}^k. \tag{19}$$

We use a total of 644 calculated MRDCI energies[17] for the fit (about three times more than in previous *ab initio* fit[31] to the CISD energies[26]). In Table III we give the parameters of the three-body term for the $^2A'$ ground state with order

TABLE I. Two-body terms of the LiFH PES.[a]

LiF		HF		LiH	
i	c_i	i	c_i	i	c_i
0	0.259060356(+02)	0	0.146251213(+02)	0	0.326698673(+02)
1	−.571402848(+00)	1	−.875424365(−02)	1	0.224436053(−01)
2	0.708433808(+00)	2	−.508168932(+01)	2	−.140464675(+01)
3	−.918329924(+00)	3	0.750286609(+01)	3	0.215282944(+01)
α_{LiF}	0.183971702(+01)	α_{LiH}	0.286994964(+01)	α_{HF}	0.308363644(+01)
$\beta^{(2)}_{\mathrm{LiF}}$	0.585612557(+00)	$\beta^{(2)}_{\mathrm{LiH}}$	0.658031223(+00)	$\beta^{(2)}_{\mathrm{HF}}$	0.104065053(+01)

[a]All coefficients in atomic units.

$M=7$ [98 linear parameters and 3 nonlinear parameters, see Eq. (19)] and root-mean-square value of 0.028 eV and a maximum deviation of 0.111 eV. We adopt as zero energy for the fit, the energy of the three separated atoms at their ground states: Li(^{2}S) + H(^{2}S) + F(^{2}P). However, in the following we refer to all the energies with respect to the reactants asymptote Li(^{2}S)+HF($^1\Sigma^+$), i.e., the zero energy is fixed at the energy of the HF minimum.

Using the preceding fit we generate contour maps of the *ab initio* PES defined by V_{ABC} in Eq. (16) (hereafter referred to as PES3) that are plotted in Fig. 1 corresponding to the 0^o, 60^o, 75^o, 90^o, 120^o and 180^o (collinear), angles of approach (θ(Li-F-H)). From this figure we can see the main characteristics of the ground state LiFH PES, such as a nonlinear transition state shifted into the exit channel or the presence of a deep well (complex) located in the reactants side. In Table IV we present a summary of the stationary points corresponding to our PES3 fit. From this table we can see that the saddle point is at 0.262 eV, only 0.008 eV higher than the ground vibrational level of the HF diatom (see Table II) indicating that the reaction can take place even at very low kinetic energies.

In Fig. 2 we present a comparison of the saddle point and the entrance channel well energies as a function of the angle θ(Li-F-H) for the three different PES1, PES2 and the present PES3, corresponding to the dotted, dashed and solid lines, respectively. The entrance channel well is very similar, both in shape and energy, for all the PES's considered. However, this is not the case if we pay attention to the saddle point energies. In fact, the *ab initio* PES1 (dotted line) and PES3 (solid line) present the same shape although shifted in energies with a near constant displacement (the greatest difference corresponds to the collinear θ angle, i.e., 180 degrees). However, the *ad hoc* PES2 presents a different shape, with very similar energies than the PES1 for θ values greater than 120 degrees and also for θ values lower than 60 degrees, and very different energies than the PES1 for θ values from 60 to 120 degrees including the transition state angle. Therefore, the *ad hoc* PES2 presents different features than those found in the unscaled *ab initio* results (the same *ab initio* points used to fit the PES1). Moreover, the subtraction of Gaussian functions used to construct the *ad hoc* PES2[32] do not modify the saddle energies for angles of approach greater than 120 degrees while, if we consider the present findings, the modification must be maximum for the collinear approach and minimum for the transition state angle, just in the opposite trend than that followed to construct the *ad hoc* PES2.

TABLE II. Vibrational eigenvalues for the free diatomic fragments for $\ell_i=0$ in eV. (All energies are referred to the minimum of the HF potential, and the LiF and LiH minimum energies are, respectively, 0.0819 and 3.400 eV). The rotational constants are 2.572, 0.168 and 0.916 meV for HF, LiF and LiH, respectively.

v_i	E^{HF}	E^{LiF}	E^{LiH}
0	0.2536	0.1374	3.4852
1	0.7436	0.2469	3.6528
2	1.2119	0.3544	3.8163
3	1.6583	0.4598	3.9753
4	2.0826	0.5632	4.1292
5	2.4847	0.6646	4.2778
6	2.8643	0.7642	4.4206
7	3.2211	0.8618	4.5571
8	3.5547	0.9576	4.6870
9	3.8647	1.0517	4.8098
10	4.1506	1.1439	4.9249

In Fig. 3 we generate contour maps as a function of the HF distance and the θ(Li-F-H) angle in the nearness of the transition state, with the LiF distance fixed at the transition state value (1.711 Å for PES1, 1.624 Å for PES2 and 1.698 Å for the present PES3), to allow for a more detailed study of the reactive features of the three PES. The energy contours are different for the three PES (see the figure caption for a detailed explanation) but the *ab initio* potentials PES1 and PES3 have a very similar shape which strongly differs from that the *ad hoc* PES2. The dynamical implications of these different shapes are to be studied in the next sections. However, we can advance that the reactivity corresponding to the PES2 must be higher than those corresponding to the PES1 and PES3, independently of the different transition state energies, because the reactants channel (plot an imaginary line cutting at $\mathbf{R}_1\approx 1$ Å in Fig. 3) in PES2 dies just before reaching the transition state angle of about 73°, while in PES1 and PES3 the reactants channels die for angles of approach lower than 65^o being the transition state angle (about 72^o in these two PES's) side located with a more difficult access for the reactants. For a better understanding of this argument we plot the transition state energy contour in Fig. 3 using dotted lines.

In Fig. 4 we present contour maps as a function of the LiF distance and the θ(Li-F-H) angle in the nearness of the

TABLE III. Three-body term of the LiFH PES.[a]

$i\ j\ k$	d_{ijk}	$i\ j\ k$	d_{ijk}	$i\ j\ k$	d_{ijk}
1 1 0	0.478684595 (+01)	2 0 3	−.705711919 (+02)	2 3 2	0.962472020 (+04)
1 0 1	0.729385704 (+00)	4 1 0	−.724837112 (+02)	2 2 3	0.653133562 (+04)
0 1 1	−.156396911 (+02)	4 0 1	−.112253321 (+03)	3 3 1	−.193077093 (+04)
1 1 1	0.132639116 (+02)	0 4 1	−.118407657 (+05)	3 1 3	0.117964604 (+04)
2 1 0	−.269964012 (+02)	0 1 4	0.596460369 (+02)	1 3 3	−.686465507 (+04)
2 0 1	−.210930936 (+01)	1 4 0	0.497387661 (+04)	4 2 1	0.712775202 (+03)
0 2 1	0.106587036 (+03)	1 0 4	−.750727332 (+02)	4 1 2	0.197622993 (+03)
0 1 2	0.174814146 (+03)	2 2 2	0.391466559 (+04)	1 4 2	−.146287815 (+05)
1 2 0	0.237158025 (+02)	3 2 1	−.120979039 (+03)	1 2 4	0.982200900 (+03)
1 0 2	−.423941830 (+00)	3 1 2	−.112278614 (+04)	2 4 1	0.139974106 (+05)
2 1 1	−.233169881 (+02)	1 3 2	−.346070726 (+04)	2 1 4	−.502881797 (+04)
1 2 1	−.600217207 (+03)	1 2 3	−.763479012 (+04)	4 3 0	−.862358982 (+02)
1 1 2	−.755939395 (+03)	2 3 1	−.522738334 (+04)	4 0 3	−.629084325 (+02)
2 2 0	0.306634456 (+03)	2 1 3	0.594817464 (+03)	0 4 3	0.439889080 (+04)
2 0 2	−.734950008 (+01)	3 3 0	0.224748367 (+04)	0 3 4	0.178631056 (+04)
0 2 2	−.363912831 (+03)	3 0 3	0.213956399 (+02)	3 4 0	−.390915476 (+04)
3 1 0	0.583491107 (+02)	0 3 3	0.219941926 (+04)	3 0 4	0.113426507 (+03)
3 0 1	0.317300063 (+02)	4 1 1	−.658409969 (+03)	5 1 1	0.347194279 (+03)
0 3 1	0.134685929 (+04)	1 4 1	0.110136079 (+05)	1 5 1	−.397270220 (+05)
0 1 3	−.527904207 (+01)	1 1 4	0.128421948 (+04)	1 1 5	0.525784165 (+04)
1 3 0	−.950064232 (+03)	4 2 0	0.400598029 (+03)	5 2 0	−.193317625 (+03)
1 0 3	0.139715468 (+02)	4 0 2	−.985792794 (+02)	5 0 2	0.570614540 (+02)
2 2 1	0.379581932 (+03)	0 4 2	0.266636830 (+03)	0 5 2	0.120635406 (+05)
2 1 2	0.132766644 (+04)	0 2 4	0.980902655 (+02)	0 2 5	−.160938477 (+04)
1 2 2	0.948956875 (+02)	2 4 0	−.661441078 (+04)	2 5 0	0.168870873 (+05)
3 1 1	0.348535974 (+03)	2 0 4	0.224980054 (+03)	2 0 5	−.384974843 (+03)
1 3 1	0.211080768 (+04)	5 1 0	0.531197782 (+02)	6 1 0	−.132778419 (+02)
1 1 3	−.510103187 (+03)	5 0 1	0.144862254 (+03)	6 0 1	−.645978627 (+02)
3 2 0	−.631369820 (+03)	0 5 1	0.207519073 (+05)	0 6 1	0.608615169 (+04)
3 0 2	0.661457533 (+02)	0 1 5	−.342480275 (+03)	0 1 6	−.261023065 (+04)
0 3 2	0.281482565 (+03)	1 5 0	−.522800362 (+04)	1 6 0	−.840648972 (+04)
0 2 3	0.197806092 (+04)	1 0 5	0.822327905 (+02)	1 0 6	0.821495977 (+02)
2 3 0	−.105743975 (+03)	3 2 2	−.490934281 (+04)		
$\beta^{(3)}_{\mathrm{LiF}}$	0.450010967 (+00)	$\beta^{(3)}_{\mathrm{HF}}$	0.121996184 (+01)	$\beta^{(3)}_{\mathrm{LiH}}$	0.826972052 (+00)

[a]All coefficients in atomic units.

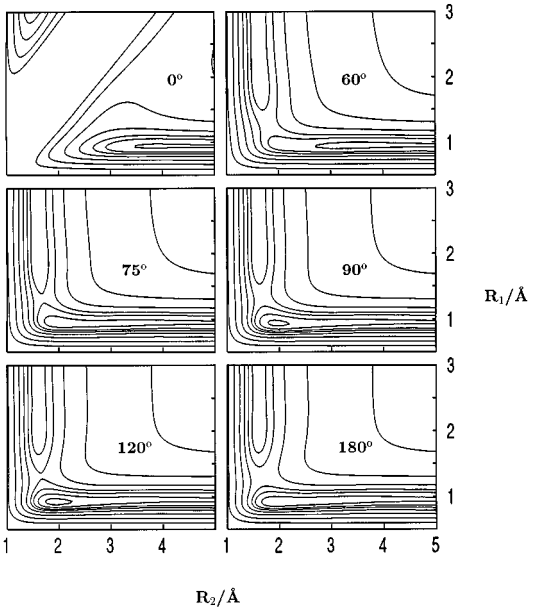

FIG. 1. Isoenergetic contours of the present Li+HF potential energy surface (PES3) with the bond angle θ(Li-F-H) fixed at 0°, 60°, 75°, 90°, 120° and 180° (collinear), plotted as a function of the HF ($\mathbf{R}_1$) and LiF ($\mathbf{R}_2$) distances (Å). The energy contours are: −0.20 (only presented for θ=120°, 90°), 0.00, 0.25, 0.50, 1.00, 2.00, 4.00 and 8.00. All the energies in eV. The zero energy is taken to be at the bottom of the asymptotic reactant well.

transition state, with the HF distance fixed at the transition state value (1.300 Å for PES1, 1.207 Å for PES2 and 1.304 Å for the present PES3). The energy contours are different for the three PES (see the figure caption for a detailed explanation) but the *ab initio* potentials PES1 and PES3 have a very similar form, with a very slight inclination towards larger LiF distances for shorter θ angles of approach that is not present when the *ad hoc* PES2 is considered. We can see also that the PES2 has the transition state shifted to shorter LiF distances.

TABLE IV. Stationary points on the LiHF PES.

	Reactants	Complex	Transition state	Second well	Products
R_{LiF} (Å)	∞	1.930	1.698	1.620	1.587
R_{HF} (Å)	0.921	0.929	1.304	1.901	∞
θ_{LiFH}	—	106.4	72.3	70.0	—
E (eV)	0.	−0.279	0.262	0.066	0.082
$E+E_0$ (eV)	0.254	—	0.328[a]	—	0.137

[a]This value corresponds to a two-dimensional approach.

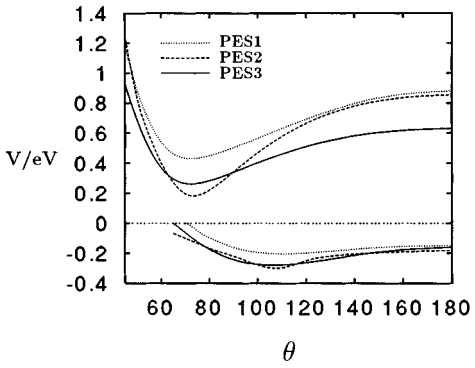

FIG. 2. Barrier heights (curves above 0.0 eV) and complex well energies (curves below 0.0 eV), plotted as a function of the bond angle θ(Li-F-H). The dotted lines are for the PES1; the dashed lines are for the PES2; and the solid lines are for the present PES3. See the text for discussion.

Since the reaction path at the saddle point nearly coincides with R_1 (see Figs. 3 and 4), the saddle zero point energies are estimated by calculating the bound states of a two-dimensional Hamiltonian of the form,

$$H=-\frac{\hbar^2}{2\mu_2}\frac{\partial^2}{\partial R_2^2}+\frac{\hbar^2\mathbf{l}_2{}^2}{2\mu_2 R_2^2}+\frac{\hbar^2\mathbf{l}_1{}^2}{2\mu_1(R_1^{\mathrm{sp}})^2}+V(R_1^{\mathrm{sp}},R_2,\theta)$$

with R_1^{sp} being the HF distance at the saddle point.

IV. RESULTS AND DISCUSSION

A. Three dimensional results

In the three dimensional calculations presented in this work $J=0$ is considered, impose that $\ell_1=\ell_2\equiv\ell$, and 16 rotational functions are used, $0\leqslant\ell_i\leqslant 15$. $\Psi_I(t)$ is described in a bidimensional radial grid formed by $n_1=210$ and $n_2=396$ equidistant points for R_1 and R_2, respectively, in the intervals $0.25\leqslant R_1\leqslant 10$ Å and $0.5\leqslant R_1\leqslant 18$ Å. The absorption parameters used are $R_1^{\mathrm{abs}}=7$ Å, $R_2^{\mathrm{abs}}=15$ Å, $\beta_1=\beta_2=0.015\text{Å}^{-2}$. The initial wave packet corresponds to the ($v_1^0=0$, $\ell_1^0=0$) eigenstate of the HF reactant and a complex gaussian located at 13 Å characterized by a mean energy of 0.0954 eV with an energy spread of 0.0318 eV. The $\Psi_P(t)$ component of the wave packet is described in a grid of $4\times n_1$ for R_1 and $8\times n_2$ for R_2 in order to improve the momentum resolution for the final probabilities as it was described above.

Some physical insight can be extracted from the analysis of the evolution of the density probability contourplots for different times, in Fig. 5. The reaction mainly takes place at ≈ 0.6 ps, with low probability. After that time the products reach very rapidly the absorption region while the portion of the probability in the reactants part flies apart much more slowly. The reason is that, first, the available kinetic energy is higher in the products channel and, second, $\mu_2\approx 5\mu_1$ what means that for the same kinetic energy the products would fly apart approximately two times faster than the reactants. As it was stressed in the previous section, the saddle point corresponds to an angular configuration of $\approx 75°$. In Fig. 6 the contourplots of the density probability for some different

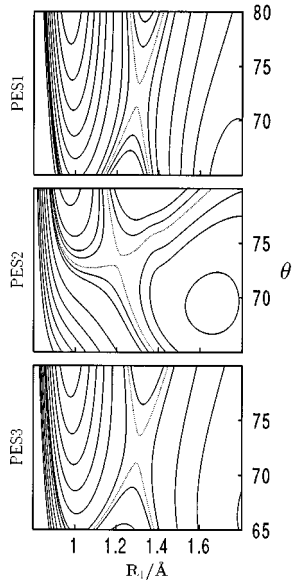

FIG. 3. Potential energy contour maps as a function of the HF ($\mathbf{R}_1$) distance (in Å) and the LiFH angle θ, with the LiF distance fixed at the transition state values for each PES. The curves are contours of the interaction potential corresponding to: 0.1, 0.15, 0.2, 0.25, 0.3, 0.35, 0.4, 0.42, 0.431 (transition state energy, marked with dotted curves), 0.44, 0.45 and 0.5 eV for the PES1 (top panel); 0.1, 0.14, 0.16, 0.17, 0.182 (transition state energy, marked with dotted curves), 0.19, 0.2, 0.25, 0.3, 0.35, 0.4, 0.45, 0.5 eV for the PES2 (intermediate panel); 0.0, 0.05, 0.1, 0.15, 0.2, 0.25, 0.262 (transition state energy, marked with dotted curves), 0.27, 0.3, 0.35, 0.4, 0.45, 0.5 eV for the present PES3 (bottom panel).

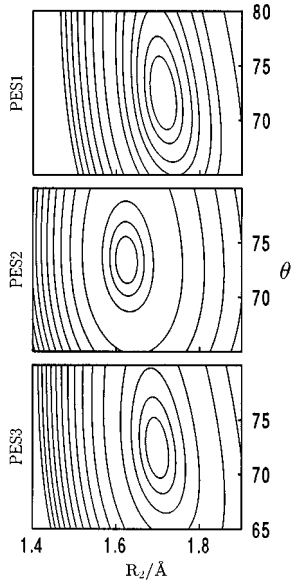

FIG. 4. Potential energy contour maps as a function of the LiF ($\mathbf{R}_2$) distance (in Å) and the LiFH angle θ, with the HF distance fixed at the transition state values for each PES. The curves are contours of the interaction potential corresponding to: 0.435, 0.44, 0.45, 0.46, 0.48, 0.5, 0.55, 0.6, 0.65, 0.7, 0.75, 0.8 and 0.85 eV for the PES1 (top panel); 0.185, 0.19, 0.20, 0.25, 0.3, 0.35, 0.4, 0.45, 0.5, 0.55, 0.6, 0.65, 0.7, 0.75, 0.8 and 0.85 eV for the PES2 (intermediate panel); 0.265, 0.27, 0.28, 0.3, 0.35, 0.4, 0.45, 0.5, 0.55, 0.6, 0.65, 0.7, 0.75, 0.8 and 0.85 eV for the present PES3 (bottom panel).

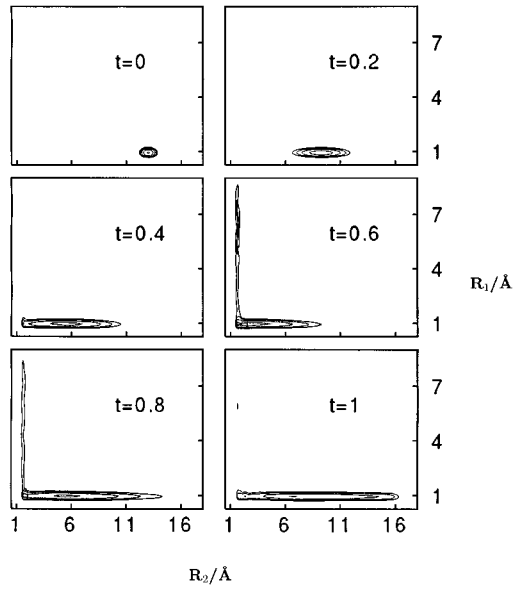

FIG. 5. Snapshots of the density probability contourplots, $P(R_1, R_2, t)=\Sigma_{\ell}|\Phi_{\ell,\ell}(R_1, R_2, t)|^2$, for different times (in ps).

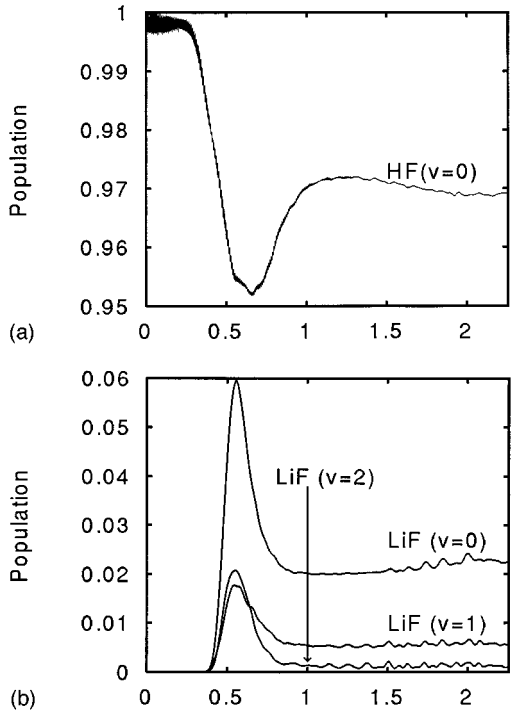

FIG. 7. Vibrational populations of the diatomic fragments vs time ($P_{v_\alpha}(t)=\Sigma_{\ell_\alpha} P_{v_\alpha \ell_\alpha}(t)$): (a) for $v_1=0$ of HF; (b) for $v_2=0,1,2$ of LiF.

angular configurations are shown which are obtained using the spherical harmonic addition theorem[61] as,

$$P(R_1, R_2, \theta, t) = \left| \sum_{\ell} (-1)^{\ell} \frac{\sqrt{2\ell+1}}{4\pi} P_{\ell}(\cos\theta)\Phi_{\ell\ell}(R_1, R_2, t) \right|^2, \tag{20}$$

where $P_{\ell}(\cos\theta)$ is a Legendre polynomial. It is observed that the reaction mainly takes place through the interval $60° \leqslant \theta \leqslant 90°$. Such narrow reaction path may explain, in part, the low reaction probability.

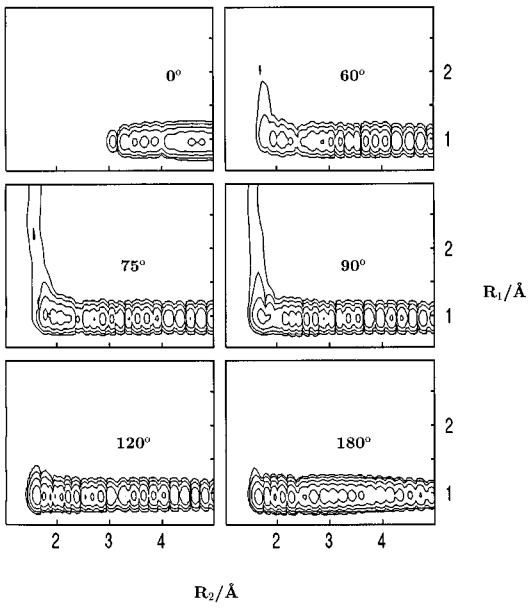

FIG. 6. Snapshots of the density probability contourplots, for different angular configurations at $t=0.6$ ps.

More detailed information about the reaction is extracted from the time evolution of the decomposition of the total wave packet on the final states of the diatomic fragments, shown in Figs. 7. The oscillations of the population of HF ($v_1=0$) at short time, Fig. 7a, are due to the kinetic crossing term which mixes the first two vibrational and few rotational states of HF since in these coordinates the eigenstates of the diatomic fragments are not purely asymptotic states of the triatomic Hamiltonian. However, the mixing occurring at so large distances between the reactants eigenstates is small, of the order of 0.3%, because the central F atom is the heavier one and the kinetic energy considered is quite low. Assuming this small mixing to be of the order of the error made, the transformation to the reactants/products Jacobi coordinates is not performed since it would increase significantly the computational effort. The final populations of the LiF products, in Fig. 7b, are rather low, $\approx$3%, and the major contribution corresponds to $v_2=0$. This result is in qualitative agreement with the experimental results obtained at comparable energies[2] in which the reactive cross section is rather small, ≈ 0.9 Å^2, and the final states of the LiF products were assigned only to $v_2=0$.

The propagation in time has been performed up to 3 ps and for this time $\approx$87% of $|\Psi_I(t)|^2$ is absorbed. As it was discussed above, the portion of the wave packet remaining in the interaction region corresponds to the reactant channel. The S^2 matrix elements for the reaction, in Fig 8, are converged better than 1% as a function of time. The reaction

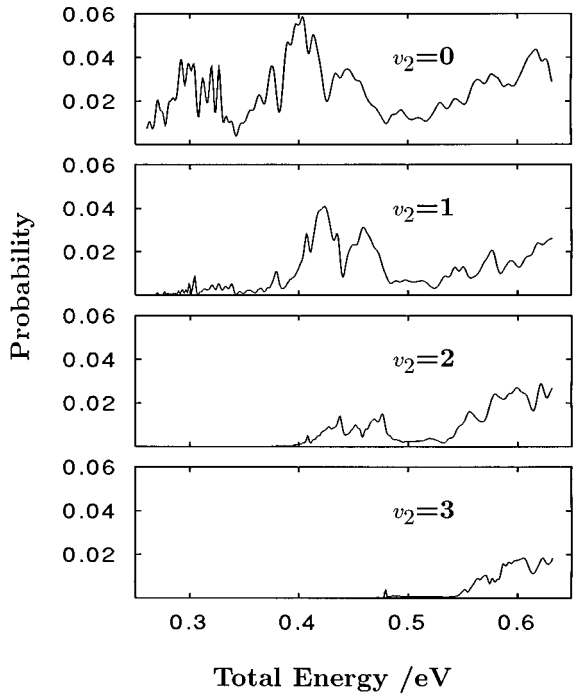

FIG. 8. Reaction probabilities summed over ℓ_2 for the Li+HF(v_1=0, ℓ_1=0, J=0) →LiF(v_2=0,1,2,3)+H reaction vs total energy.

probabilities thus obtained are rather lower than those recently reported[32,36,37] using the PES2. Such difference cannot be only attributed to the height of the saddle point, since the potential used in this work is only ≈0.08 eV higher. Furthermore, the addition of the zero-point energies at the saddle point (≈0.067 eV and ≈0.103 eV, for PES3 and PES2, respectively), even reduce this difference to ≈0.03 eV. Therefore, the big difference in the reaction probabilities when using these two potential surfaces is attributed to different topological features at the saddle point, in particular, to its position with respect to the entrance channel (see Fig. 3). This fact will be discussed in more detail in the next section.

The estimated zero-point energy can also explain why the reaction probabilities for a particular final vibrational state have significant values about 0.05–0.1 eV after the opening of the channel. Assuming that the reaction takes place adiabatically from the reactants directly to the corresponding final state of LiF, such a shift may be attributed to the zero-point energy of the reaction in the saddle point.

The energy structure of the reaction probabilities in Fig. 8 shows sharp peaks superimposed to a slow oscillating envelope, qualitatively similar to those previously obtained.[32,37] The main difference comes from the intensity and width of the peaks attributed to resonances. In previous calculations, using local coordinates in the IOS approximation[35] on this system with the PES2 some of the sharp resonances were attributed to quasibound states for which the energy is temporarily trapped in a transverse Li-F vibrational motion between the saddle point and a second barrier present in the product valley. In the PES3 used in this work there is a minimum in the products valley after the saddle point but the second maximum is absent as it seems to indicate previous *ab initio* calculations.[17] Therefore, the resonances due to quasibound states trapped in the products minimum are expected to have broader widths.

B. Two dimensional results

Since the reaction path in the saddle point nearly coincides with R_1 it is expected that the reaction is more efficiently produced when the energy is localized in the HF vibration than in translational motion between the two reactants. In addition it is interesting to compare with the previous PES2 of Ref. 32 since in this surface the reaction is already very efficient for HF initially in its ground vibrational level. Due to the high computational effort required in three-dimensional calculations, it is convenient to reduce the dimensionality of the problem. For that purpose two approximations will be assumed in what follows. First, the kinetic crossing term is neglected since the central F atom is the heavier one. Second, the interaction potential is assumed to be isotropic and equal to the minimum value of the full potential, V_{ABC} for each R_1 and R_2 configuration in order to maintain the main energetic features of the process studied. With these two approximations, the rotational labels, $[\ell_1, \ell_2]$, become good quantum numbers all along the collision process, and in the two-dimensional calculations only $\ell_1=\ell_2=0$ are included. A larger radial grid than that for the 3D calculation have been used, formed by 384 and 672 equidistant points for R_1 and R_2, respectively, in the intervals $0.25 \leqslant R_1 \leqslant 18$ Å and $0.5 \leqslant R_2 \leqslant 23.5$ Å. Two different calculations have been performed, for initial HF(v_1=0,1). For v_1=0 the initial complex gaussian has a mean kinetic energy of 0.585 eV while for v_1=1 it is of 0.217 eV, and in the two cases the energy spread is one third of the mean kinetic energy. Therefore, the reaction probabilities for these two different vibrational excitations of the HF reactant can be compared in the [0.8, 1.2] eV energy range.

All the calculations presented in what follows have been propagated until >99.9 % of the probability has been absorbed. All the possible S^2 matrix elements have been computed and their sum is very close to unity with an upper error limit of ≈2% for PES1 and PES3. Such error mainly occurs in the vicinity of narrow resonances and for lower total energies, which in general have small contributions in the total energy distribution and because the corresponding components in the asymptotic region converge more slowly with time. For the PES1 and PES3 the S^2 matrix elements obtained using Eq. (15) were in very good agreement with those obtained using the method proposed by Balint-Kurti *et al.*[35,37,62] However, for the PES2 the agreement was worse because very narrow resonances were obtained and the method based in a momentum grid, of Eq. (15), would require a much dense grid to resolve the resonances. In the vicinity of narrow resonances, the method of Balint-Kurti *et al.*[35,37,62] yielded, in general, better value of the sum of all S^2 matrix elements. The case of HF initially in v_1=1 and using PES2 has been found to be particularly problematic

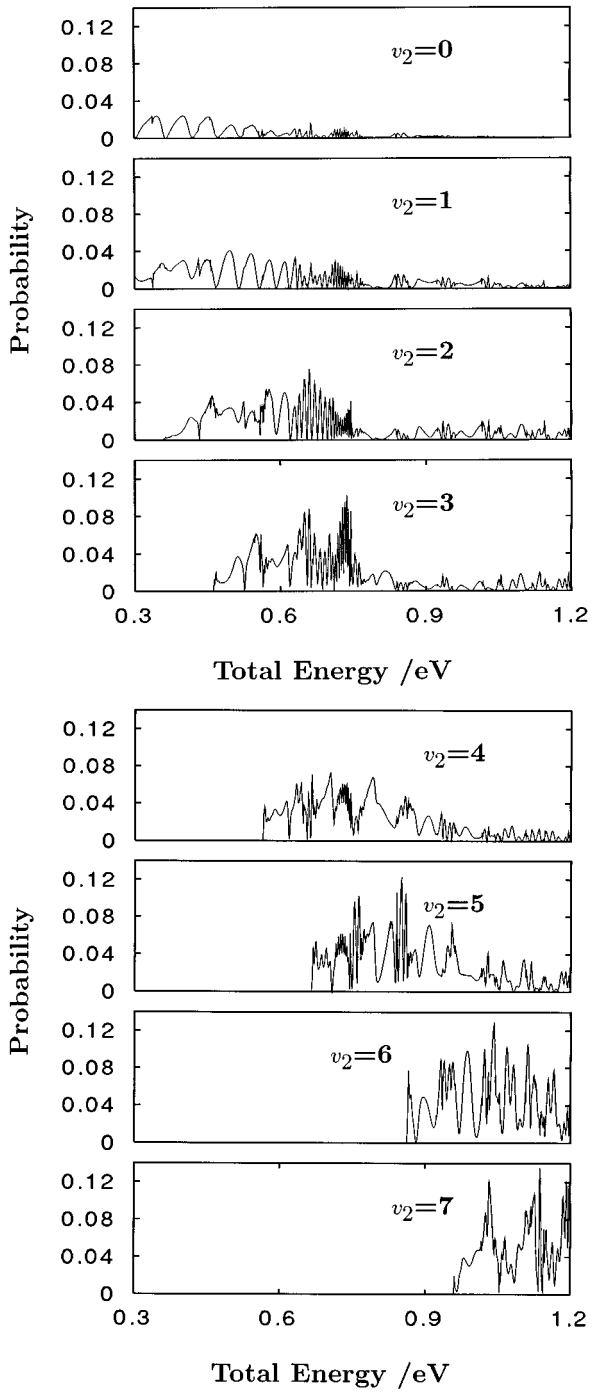

FIG. 9. Reaction probability for the Li+HF(v_1=0) →LiF(v_2)+H collision (in two dimensions) for the PES3.

because for some energetic regions close to narrow resonances the sum of all possible S^2 matrix elements could have an error of the order of 15%. This will be commenteded on in what follows.

The reaction probabilities for HF(v_1=0) as a function of the final vibrational states of the LiF(v_2) products, and using the PES3, are shown in Fig. 9. The total reaction probability is very close, in magnitude, to that obtained in the three-dimensional treatment (in Fig. 8). However, the 2D approach used here seems to produce larger vibrational excitation in the final LiF products than the 3D treatment. Another difference is the frequency and amplitude of the background oscillating envelope. Such oscillations were explained as a quantum interference effect between the reactant and product channels[32] and it was also found that the interference patterns were different to those obtained in previous 2D calculations,[35] as it is the case between the 3D and 2D calculations presented in this work for the PES3. In the simple model of Ref. 32 the frequency of the oscillations depends on the energy mismatch between the reactant and product channels. Since in the 2D approach the rotational excitations are eliminated, such energy difference increases, what produces an increase of the frequency of the oscillations of the reaction probabilities when compared to the 3D results. In addition, as the energy mismatch increases in the simple model, the overlap between the reactant and product wave functions decreases what produces a decrease of the effective coupling between them and, therefore, the amplitude of the oscillation decreases too.

The reaction probabilities for different final vibrational states of the LiF(v_2) products, obtained for the PES2 and using the 2D approach described above, are shown in Fig. 10. These calculations were done previously[35] and are repeated here to avoid discrepancies due to differences between the two 2D approaches. In fact, the results presented in Fig. 10 compares very nicely with those shown in Figs. 5–8 of Ref. 35. The main difference is that in the present bidimensional approach the final vibrational excitation of the LiF products is higher than in Ref. 35. Since a similar effect was observed between the 3D and 2D results using the PES3 it may be concluded that the present bidimensional approach overestimates the final vibrational excitation of the LiF products.

The comparison of Figs. 9 and 10 clearly shows very different reactivity on the two potential surfaces. First of all, for the PES2 the final vibrational level of LiF most efficiently populated is v_2=0 while for the PES3 the vibrational distribution peak is shifted to $v_2 \approx 5$. However, for low energies the 3D treatment indicates that the two potential surfaces yield a major final vibrational state of LiF products in v_2=0, in agreement with the available experimental data.[2] Another important difference between the results obtained for the two potential surfaces in the 2D treatment is that the total reaction probability is higher than 90% for the PES2 of Ref. 32 in nearly all the energy range while for the PES3 it never reaches higher than 30% (see Fig. 11).

In order to determine the reason of the different reactivity when using PES2 and PES3 we have performed calculations on a third potential surface, PES1, and the total reaction probabilities are shown in Fig. 11. The PES1 is characterized by a higher barrier, ≈0.433 eV, than PES3 or PES2 and in the vicinity of the saddle point PES1 looks very similar to PES3 (see Fig. 3). The total reaction probability for PES1 is similar to that for PES3: there is an energy shift of the order of the energy difference between the height of the barriers, ≈0.18 eV. Therefore, it may be concluded that the different reactivity of PES2 is mainly due to the shape of the potential

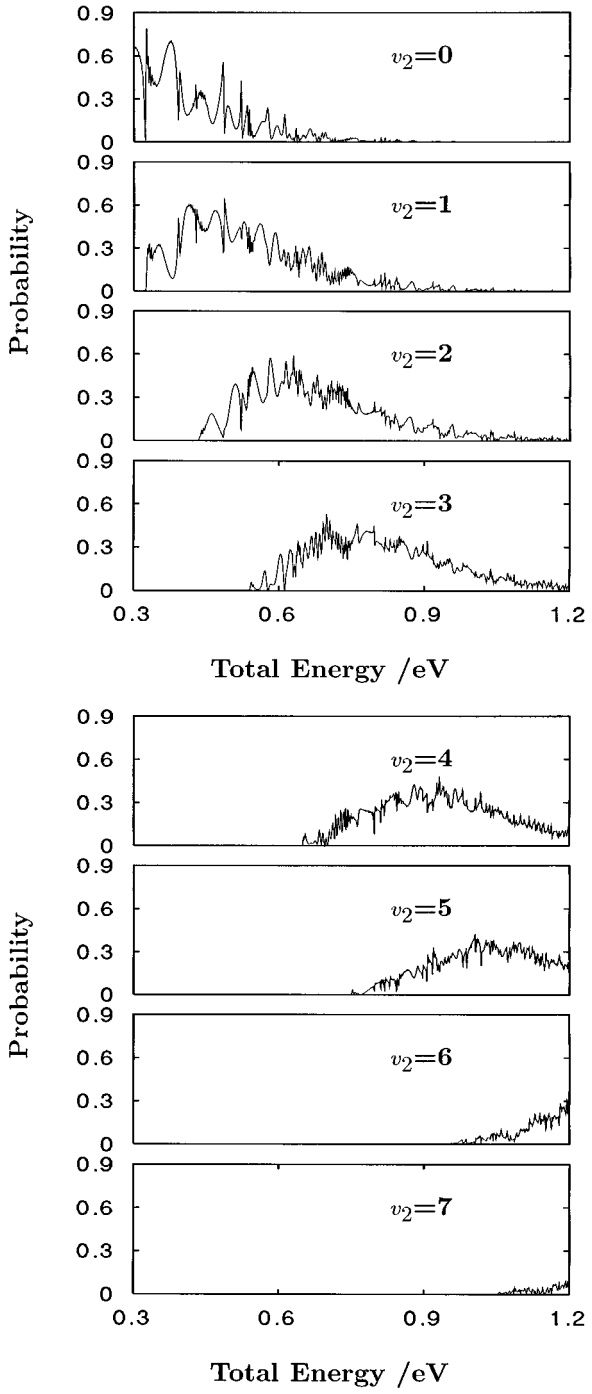

FIG. 10. Same as in Fig. 9 but using the PES2 of Ref. 32.

in the region in which the entrance channel matches the saddle point. The PES1 is obtained by fitting the *ab initio* points to an analytical form[31] and the topology of the PES is very similar to that of the PES3 but they differ in the height of the barrier and in the energetics of the diatomic fragments. Since the *ab initio* points[17] used to fit the PES3 are, in principle, more accurate than those used for PES1[26] it may be concluded that the better reaction probabilities are those obtained using PES3. However, the PES2[32] is essentially based on the same *ab initio* points[26] than PES1 but some modifications were included to diminish the height of the barrier. Such modifications alter the topology of the PES close to the saddle point and originate a second barrier in the products valley of a similar height, than produces an increase in the reactivity for $v_1=0$ and the apparition of very sharp resonances.

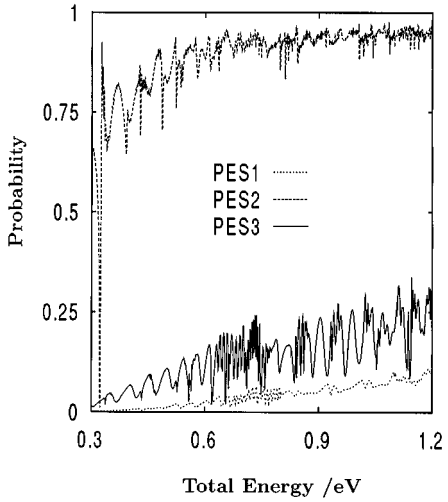

FIG. 11. Total reaction probability for the Li+HF($v_1=0$) →LiF+H collision (in two dimensions) using three different potential energy surfaces.

The total reaction probabilities for HF initially in $v_1=1$, shown in Fig. 12, are very similar for the three PES's used and very close to 95%. [The HF(v_1) eigenvalue for the PES1 is slightly higher than the other two.] The reaction probability for the PES2 shows important resonance structures which are, again, attributed to the presence of a second barrier in the products channel. The upper limit error for the PES2 is of the order ≈3% except in the vicinity of some Fano-type resonances at ≈0.854, 0.954, 1.05 and 1.13 eV, respectively. These resonances are nearly equally spaced as it was observed previously for $v_1=0$ using PES2.[35] The propagation in this case was performed until 4 ps and 99.9%

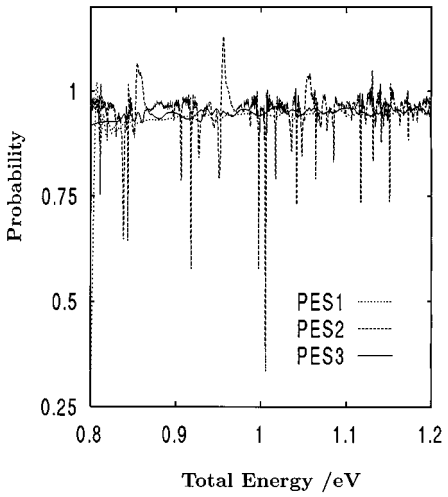

FIG. 12. Same as in Fig. 11 but for initial HF($v_1=1$).

of the population was absorbed. The S^2 matrix elements have not converged close to these resonances probably because longer times are required to resolve such narrow resonances. However, the overall behavior of the reaction probability is close to those obtained for PES1 and PES3. For the PES3 and PES1 there is an important increasing in the reactivity when increasing the vibrational energy of the reactants. Such behavior corresponds to the case of a ''late barrier.''[63] The situation is even more dramatic for the PES2 in which the zero-point vibrational energy of the HF($v_1=0$) reactant is enough to produce the reaction with a high efficiency. From the comparison of the dynamics on these three PES's it may be concluded that the position of the barrier with respect to the entrance channel is more important than the exact height of the barrier, since it is very close to the zero-point energy of the HF($v_1=0$) reactants.

V. CONCLUSIONS

In this work an analytic fit of the most accurate *ab initio* points[17] on the potential energy surface of the LiFH system is presented and the reaction dynamics is studied using a time-dependent treatment based on local coordinates. The three-dimensional wave packet calculations performed indicates that the reactivity for the HF reactant in its ground vibrational state is quite low, in contradiction with previous calculations[32,36,37] using a different potential energy surface.[32] The differences with previous potential energy surfaces are further analyzed using a restricted dimensionality approach, and it is concluded that the reason of the discrepancies is the different shape of the potential in the vicinity of the barrier rather than the ''exact'' height of the barrier.

All *ab initio* points,[17,26] suggest the same shape of the PES in the neighborhood of the transition state. In the present fit such shape has been maintained while in the preceding fit by Parker *et al.*,[32] to less accurate *ab initio* points,[26] was modified to get a lower barrier to reaction. This *ad hoc* change yielded a very much higher reaction probability for the HF reactants in the ground vibrational state and also spurious resonances have been obtained due to the appearance of an artificial minimum in the products channel. On the contrary, the present fit yields a very small reaction probability for HF($v_1=0$). At present no direct comparison with experimental data is possible, it would be necessary to perform calculations at higher total angular momentum, work which is in progress nowadays. Also, QCT calculations on the present PES are in progress[64] to fully characterize the dynamics of the Li + HF reaction at the collision energies and rovibrational numbers needed to simulate the experimental results.

Nevertheless, the experimental total cross section for this reaction with the HF reactants in the ground vibrational state is rather low[2] as our calculations predict. Moreover, the reactivity of this kind of system is greatly enhanced for vibrationally excited states of the reactants,[65,66] in qualitative agreement with the reduced dimensionality calculations presented in this work. To conclude, the present PES fit, being the most accurate currently available, is also expected to be in better agreement with the experiment.

Since the reactivity is rather low for HF($v_1=0$) it is expected that the LiFH complex could be formed in a supersonic beam expansion, as it is the case for some related systems,[14,15] and the reaction studied after an infrared photon excitation since the dipole moment on this system is rather important.[17] The products formed during the expansion are expected to be vibrationally cold and therefore the reaction could be followed by examining the vibrationally excited states of LiF. At present, the dipole moment is being calculated to perform such study theoretically and the new *ab initio* points thus obtained will be used to improve the present ground-state potential energy surface fit.

Theoretical information of the excited-state PESs provides an opportunity for designing new experiments for transition state spectroscopy.[67,68] Recently,[17] we have proposed a laser-catalyzed Li+HF reaction based on low electronic excited-state calculations. The process may be as follows:[18] (a) starts by forming a complex Li···FH on the ground state, (b) is excited by visible or near-infrared light to one of the lower excited states (excited-state complex LiFH*), and (c) after moving across that potential hops back to the ground state to give products. At an early date we can provide fits of the excited-state PESs and transition dipoles needed to perform the corresponding dynamical treatment of this proposed laser-catalyzed Li + HF reaction.

ACKNOWLEDGMENTS

This work has been supported by DGICYT (Ministerio de Educación y Ciencia, Spain) under Grant Nos. PB94-0160 and PB92-0053. Special thanks are due to Professor Francisco Javier Aoiz and Dr. Marta I. Hernández for very helpful discussions. We also want to acknowledge DGICYT and CIEMAT for the use of a CRAY-J90.

[1] E. H. Taylor and S. Datz, J. Chem. Phys. **23**, 1711 (1955).
[2] C. H. Becker, P. Casavecchia, P. W. Tiedemann, J. J. Valentini, and Y. T. Lee, J. Chem. Phys. **73**, 2833 (1980).
[3] M. Hoffmeister, R. Schleysing, F. Stienkemeier, and H. J. Loesch, J. Chem. Phys. **90**, 3528 (1989).
[4] H. J. Loesch, E. Stenzel, and B. Wüstenbecker, J. Chem. Phys. **95**, 3841 (1991).
[5] H. J. Loesch and F. Stienkemeier, J. Chem. Phys. **98**, 9570 (1993).
[6] H. J. Loesch and F. Stienkemeier, J. Chem. Phys. **99**, 9598 (1993).
[7] T. F. George, J. Yuan, and I. H. Zimmermann, Faraday Discuss. Chem. Soc. **62**, 246 (1977).
[8] J. C. Light and A. Altenberger–Siczek, J. Chem. Phys. **70**, 4108 (1979).
[9] A. E. Orel and W. H. Miller, J. Chem. Phys. **70**, 4393 (1979).
[10] K. C. Kulander and A. E. Orel, J. Chem. Phys. **74**, 6529 (1981).
[11] K. C. Kulander and A. E. Orel, J. Chem. Phys. **75**, 675 (1981).
[12] M. Shapiro and Y. Zeiri, J. Chem. Phys. **85**, 6449 (1986).
[13] T. Seideman and M. Shapiro, J. Chem. Phys. **88**, 5525 (1988).
[14] B. Soep, C. J. Whitham, A. Keller, and J. P. Visticot, Faraday Discuss. Chem. Soc. **91**, 191 (1991).
[15] B. Soep, S. Abbés, A. Keller, and J. P. Visticot, J. Chem. Phys. **96**, 440 (1992).
[16] S. K. Shin, Y. Chen, S. Nckolaisen, S. W. Sharpe, R. A. Beaudet, and C. Wittig, Adv. Photochem. **16**, 249 (1991).
[17] A. Aguado, C. Suárez, and M. Paniagua, Chem. Phys. **201**, 107 (1995).
[18] J. C. Polanyi and X.-Y. Chang (private communication).
[19] B. Soep (personal communication).
[20] Y. Zeiri and M. Shapiro, Chem. Phys. **31**, 217 (1978).

[21] M. Shapiro and Y. Zeiri, J. Chem. Phys. **70**, 5264 (1979).
[22] G. G. Balint-Kurti and R. N. Yardley, Faraday Discuss. Chem. Soc. **62**, 77 (1977).
[23] M. Paniagua and A. Aguado, Chem. Phys. **134**, 287 (1989).
[24] C. Suárez, A. Aguado, C. Tablero, and M. Paniagua, Int. J. Quantum Chem. **52**, 935 (1994).
[25] W. A. Lester, Jr. and M. Krauss, J. Chem. Phys. **52**, 4775 (1970).
[26] M. M. L. Chen and H. F. Schaefer III, J. Chem. Phys. **72**, 4376 (1980).
[27] C. Suárez, A. Aguado, and M. Paniagua, Chem. Phys. **178**, 357 (1993).
[28] S. Carter and J. N. Murrell, Mol. Phys. **41**, 567 (1980).
[29] E. García and A. Laganà, Mol. Phys. **52**, 1115 (1984).
[30] A. Laganà, O. Gervasi, and E. García, Chem. Phys. Lett. **143**, 174 (1988).
[31] A. Aguado and M. Paniagua, J. Chem. Phys. **96**, 1265 (1992).
[32] G. A. Parker, A. Laganà, S. Crocchianti, and R. T. Pack, J. Chem. Phys. **102**, 1238 (1995).
[33] R. B. Walker, Y. Zeiri, and M. Shapiro, J. Chem. Phys. **74**, 1763 (1981).
[34] J. M. Alvariño, M. L. Hernández, E. García, and A. Laganà, J. Chem. Phys. **84**, 3059 (1986).
[35] G. G. Balint-Kurti, F. Gögtas, S. P. Mort, A. R. Offer, A. Laganà, and O. Gervasi, J. Chem. Phys. **99**, 9567 (1993).
[36] M. Baer, I. Last, and H.-J. Loesch, J. Chem. Phys. **101**, 9648 (1994).
[37] F. Gögtas, G. G. Balint-Kurti, and A. R. Offer, J. Chem. Phys. **104**, 7927 (1996).
[38] R. S. Judson, D. J. Kouri, D. Neuhauser, and M. Baer, Phys. Rev. A **42**, 351 (1990).
[39] D. H. Zhang and J. Z. H. Zhang, J. Chem. Phys. **101**, 3672 (1994).
[40] D. H. Zhang and J. Z. H. Zhang, J. Chem. Phys. **101**, 1146 (1994).
[41] D. H. Zhang, J. Z. H. Zhang, Y. Zhang, D. Wang, and Q. Zhang, J. Chem. Phys. **102**, 7400 (1995).
[42] E. M. Goldfield, S. K. Gray, and G. C. Schatz, J. Chem. Phys. **102**, 8807 (1995).
[43] D. H. Zhang and J. Z. H. Zhang, J. Chem. Phys. **103**, 6512 (1995).
[44] D. H. Zhang and J. C. Light, J. Chem. Phys. **104**, 4544 (1996).
[45] S. Carter and N. C. Handy, Mol. Phys. **47**, 1445 (1982).
[46] S. Carter, N. C. Handy, and B. T. Sutcliffe, Mol. Phys. **49**, 745 (1983).
[47] J. R. Reimers and R. O. Watts, Mol. Phys. **52**, 357 (1984).
[48] G. A. Natanson, S. Ezra, G. Delgado-Barrio, and R. S. Berry, J. Chem. Phys. **81**, 3400 (1984).
[49] G. A. Natanson, S. Ezra, G. Delgado-Barrio, and R. S. Berry, J. Chem. Phys. **84**, 2035 (1986).
[50] P. Villarreal, O. Roncero, and G. Delgado-Barrio, J. Chem. Phys. **101**, 2217 (1994).
[51] M. von Dirke, B. Heuman, R. Schinke, R. J. Sension, and B.S. Hudson, J. Chem. Phys. **99**, 1050 (1993).
[52] R. N. Dixon, C. C. Marston, and G. G. Balint-Kurti, J. Chem. Phys. **93**, 6520 (1990).
[53] B. Heuman, K. Weide, R. Dran, and R. Schinke, J. Chem. Phys. **98**, 5508 (1993).
[54] R. Schinke and V. Engel, J. Chem. Phys. **93**, 3252 (1990).
[55] E. J. Heller, J. Chem. Phys. **62**, 1544 (1975).
[56] R. Metiu and Horia Metiu, J. Chem. Phys. **86**, 5009 (1987).
[57] P. Pernot and W. A. Lester, Jr., Int. J. Quantum Chem. **40**, 577 (1991).
[58] H. Tal-Ezer and R. Kosloff, J. Chem. Phys. **81**, 3967 (1984).
[59] W. H. Press, S. A. Teukolsky, W. T. Vetterling, and B. P. Flannery, *Numerical Recipes* (Cambridge University Press, Cambridge, 1994).
[60] A. J. C. Varandas, Adv. Chem. Phys. **74**, 255 (1988).
[61] R. N. Zare, *Angular Momentum* (Wiley, New York, 1988).
[62] G. G. Balint-Kurti, R. N. Dixon, and C. C. Marston, J. Chem. Soc. Faraday Trans. **86**, 1741 (1990).
[63] J. C. Polanyi and W. H. Wong, J. Chem. Phys. **51**, 1439 (1969).
[64] F. J. Aoiz (personal communication, 1996).
[65] T. J. Odiorne, P. R. Brooks, and J. V. V. Kasper, J. Chem. Phys. **55**, 1980 (1971).
[66] Z. Karny and R. N. Zare, J. Chem. Phys. **68**, 3360 (1978).
[67] K. Liu, J. C. Polanyi, and S. Yang, J. Chem. Phys. **98**, 5431 (1993).
[68] J. C. Polanyi and J.-X. Wang, J. Phys. Chem. **99**, 13691 (1995).